



## Diurnal variations of BrONO<sub>2</sub> observed by MIPAS-B at midlatitudes and in the Arctic

Gerald Wetzel<sup>1</sup>, Hermann Oelhaf<sup>1</sup>, Michael Höpfner<sup>1</sup>, Felix Friedl-Vallon<sup>1</sup>, Andreas Ebersoldt<sup>2</sup>, Thomas Gulde<sup>1</sup>, Sebastian Kazarski<sup>1</sup>, Oliver Kirner<sup>3</sup>, Anne Kleinert<sup>1</sup>, Guido Maucher<sup>1</sup>, Hans Nordmeyer<sup>1</sup>, Johannes Orphal<sup>1</sup>, Roland Ruhnke<sup>1</sup>, and Björn-Martin Sinnhuber<sup>1</sup>

<sup>1</sup>Karlsruhe Institute of Technology, Institute of Meteorology and Climate Research, Karlsruhe, Germany

<sup>2</sup>Karlsruhe Institute of Technology, Institute for Data Processing and Electronics, Karlsruhe, Germany

<sup>3</sup>Karlsruhe Institute of Technology, Steinbuch Centre for Computing, Karlsruhe, Germany

Correspondence to: Gerald Wetzel (gerald.wetzel@kit.edu)

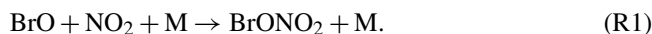
Received: 4 May 2017 – Discussion started: 19 May 2017

Revised: 20 September 2017 – Accepted: 6 November 2017 – Published: 7 December 2017

**Abstract.** The first stratospheric measurements of the diurnal variation in the inorganic bromine (Br<sub>y</sub>) reservoir species BrONO<sub>2</sub> around sunrise and sunset are reported. Arctic flights of the balloon-borne Michelson Interferometer for Passive Atmospheric Sounding (MIPAS-B) were carried out from Kiruna (68° N, Sweden) in January 2010 and March 2011 inside the stratospheric polar vortices where diurnal variations of BrONO<sub>2</sub> around sunrise have been observed. High nighttime BrONO<sub>2</sub> volume mixing ratios of up to 21 pptv (parts per trillion by volume) were detected in late winter 2011 in the absence of polar stratospheric clouds (PSCs). In contrast, the amount of measured BrONO<sub>2</sub> was significantly lower in January 2010 due to low available NO<sub>2</sub> amounts (for the build-up of BrONO<sub>2</sub>), the heterogeneous destruction of BrONO<sub>2</sub> on PSC particles, and the gas-phase interaction of BrO (the source to form BrONO<sub>2</sub>) with ClO. A further balloon flight took place at midlatitudes from Timmins (49° N, Canada) in September 2014. Mean BrONO<sub>2</sub> mixing ratios of 22 pptv were observed after sunset in the altitude region between 21 and 29 km. Measurements are compared and discussed with the results of a multi-year simulation performed with the chemistry climate model ECHAM5/MESy Atmospheric Chemistry (EMAC). The calculated temporal variation in BrONO<sub>2</sub> largely reproduces the balloon-borne observations. Using the nighttime simulated ratio between BrONO<sub>2</sub> and Br<sub>y</sub>, the amount of Br<sub>y</sub> observed by MIPAS-B was estimated to be about 21–25 pptv in the lower stratosphere.

### 1 Introduction

Chlorine and bromine species play a dominant role in the contribution to ongoing stratospheric ozone depletion since the amount of equivalent effective stratospheric chlorine (chlorine and bromine) is predicted to return to 1980 values by 2050 at midlatitudes (Newman et al., 2007; Stolarski et al., 2010). BrONO<sub>2</sub> is the most abundant inorganic bromine (Br<sub>y</sub>) compound in the stratosphere, besides BrO (see, e.g., Brasseur and Solomon, 2005; Sinnhuber et al., 2009; Sinnhuber and Meul, 2015). BrONO<sub>2</sub> is formed via the reaction with BrO and NO<sub>2</sub>:



During the day, BrONO<sub>2</sub> is photolysed with different possible channels:



with a higher quantum yield of Reaction (R2a) compared to Reaction (R2b). BrONO<sub>2</sub> can also be destroyed via the reaction with atomic oxygen:

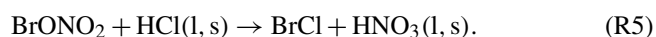


Reactions (R1) to (R3) show the close connection between BrO and BrONO<sub>2</sub> leading to an opposite diurnal variation in these species. Gas-phase BrONO<sub>2</sub> can also be converted

**Table 1.** Overview of MIPAS balloon flights and number of limb sequences recorded around sunrise (Kiruna) and sunset (Timmins). Measurement times are given in UTC and local solar time (LST) together with the solar zenith angle (SZA). Latitude and longitude refer to the tangent points of the observations.

| Location | Date         | UTC         | LST         | SZA (deg)  | Seq. no. | Latitude (° N) | Longitude (° E) |
|----------|--------------|-------------|-------------|------------|----------|----------------|-----------------|
| Kiruna   | 24 Jan 2010  | 06:17–10:21 | 08:13–12:36 | 98.1–86.2  | 19       | 69.3–66.9      | 28.8–33.7       |
| Kiruna   | 31 Mar 2011  | 02:00–04:38 | 04:01–06:34 | 99.4–83.1  | 12       | 64.0–63.5      | 30.1–28.9       |
| Timmins  | 7–8 Sep 2014 | 21:40–02:33 | 16:25–21:00 | 69.9–115.1 | 37       | 45.9–46.2      | –78.8– –83.2    |

to gas-phase HOBr and BrCl on sulfate aerosols and polar stratospheric cloud (PSC) particles where H<sub>2</sub>O, HCl, and HNO<sub>3</sub> are in liquid (l) or solid phase (s):



An interaction between the chlorine and bromine family (particularly important at high latitudes in winter under conditions of elevated ClO) is the gas-phase production of BrCl via



Stratospheric BrONO<sub>2</sub> was detected for the first time by the Michelson Interferometer for Passive Atmospheric Sounding (MIPAS) aboard the Envisat satellite (Höpfner et al., 2009). Strong day or night variations were observed with much lower concentrations during the day compared to nighttime. A maximum amount of 20–25 pptv (parts per trillion by volume) was inferred from MIPAS spectra recorded during the night.

Flights of the balloon version of the MIPAS instrument (MIPAS-B) investigated in this work were carried out from Kiruna (68° N, Sweden) on 24 January 2010 and 31 March 2011 as well as from Timmins (49° N, Canada), on 7–8 September 2014. For the first time, diurnal variations of BrONO<sub>2</sub> around sunrise (Kiruna flights) and sunset (Timmins flight) were measured by MIPAS-B with a high temporal resolution. A description of the MIPAS-B instrument, data analysis, and chemical modelling is given in Sect. 2. A discussion of observed BrONO<sub>2</sub> volume mixing ratio (VMR) vertical profiles follows in Sect. 3 together with a comparison of the measured data to simulations of the chemistry climate model ECHAM5/MESy Atmospheric Chemistry (EMAC) to check the current understanding of stratospheric bromine chemistry and to estimate the amount of lower-stratospheric Br<sub>y</sub>.

## 2 MIPAS-B instrument, data analysis, and modelling

In the following sections, we give an overview of the MIPAS-B instrument and the balloon flights together with the corresponding data analysis and a description of chemical modelling performed for this study.

### 2.1 MIPAS-B instrument and balloon flights

The balloon-borne cryogenic Fourier transform limb emission spectrometer operates in the mid-infrared spectral region between about 4 and 14 μm. The maximum optical path difference of 14.5 cm of the beam in the interferometer correlates with 0.0345 cm<sup>-1</sup> spectral resolution. This corresponds to about 0.07 cm<sup>-1</sup> after apodization with the Norton and Beer (1976) “strong” function and allows the separation of individual spectral lines from continuum-like emissions. Noise equivalent spectral radiance (NESR) values for a single calibrated spectrum are typically within 1 × 10<sup>-9</sup> and 7 × 10<sup>-9</sup> W(cm<sup>2</sup> sr cm<sup>-1</sup>)<sup>-1</sup>. A reduction in spectral noise by a factor of *n*<sup>-0.5</sup> is obtained by recording and averaging *n* spectra (*n* ≤ 16) per single elevation scan. Besides a high radiometric accuracy of typically 1 %, the pointing system allows a knowledge of the tangent altitude of better than 50 m at the 1σ confidence limit. An overview of instrument characterization in terms of the instrumental line shape, field of view, NESR, line of sight of the instrument, detector non-linearity (Kleinert, 2006), and the error assessment of the calibrated spectra is given by Friedl-Vallon et al. (2004).

In this study, we report BrONO<sub>2</sub> results from three MIPAS-B flights. Details are shown in Table 1. The first flight took place on 24 January 2010 from Kiruna over northern Scandinavia inside the Arctic vortex at the beginning of a major stratospheric warming (Wetzel et al., 2012). The second one was carried out from the same location on 31 March 2011 inside a still persistent late-winter Arctic vortex (Wetzel et al., 2015). The third one was performed at midlatitudes from Timmins (Ontario, Canada) on 7 to 8 September 2014. For this midlatitude flight, we show retrieval results from spectra observed around sunset. For the Arctic flights, MIPAS-B measurements were performed from night into day. All flights have in common that fast sequences of spectra were recorded in short time steps of about 10 min to enable the retrieval of photochemically active species, which change their concentration quickly around sunrise and sunset. The line of sight of the instrument was aligned perpendicular to the azimuth direction of the sun to allow for a symmetric illumination of the sounded air mass before and beyond the tangent point. The analysis of the recorded spectra is described in the following section.

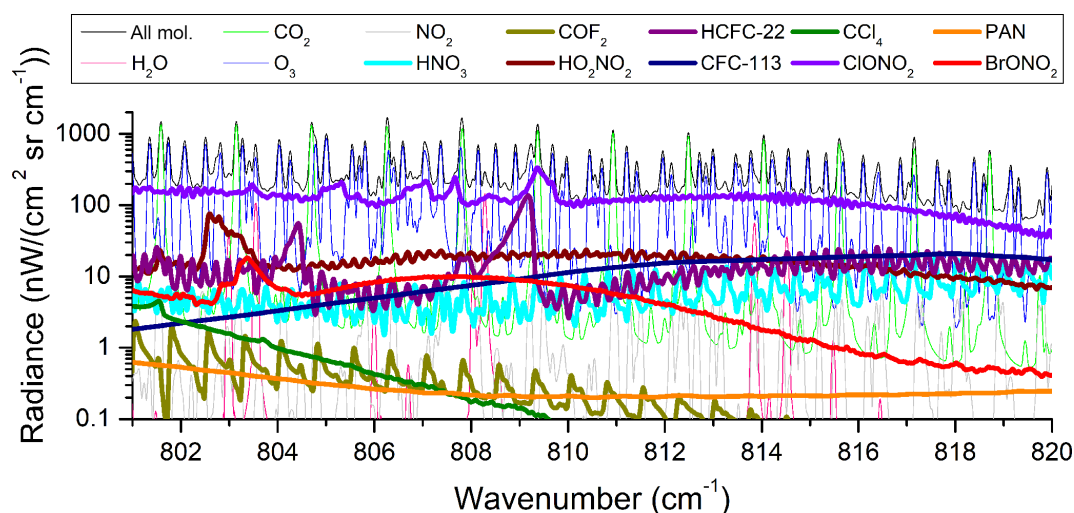


**Figure 1.** Simulated limb emission spectra (with spectral resolution of MIPAS-B) for a midlatitude summer standard atmosphere (Remedios et al., 2007) in the spectral region of the BrONO<sub>2</sub> analysis window for a tangent altitude of 20 km. Emissions of individual species contributing to the combined spectrum (all molecules, black line) are shown.

## 2.2 Data analysis

Radiance calculations were carried out with the Karlsruhe Optimized and Precise Radiative transfer Algorithm (KOPRA; Stiller et al., 2002). Spectroscopic parameters for the calculation of emission spectra were taken from the high-resolution transmission molecular absorption database (HITRAN; Rothman et al., 2009) and a MIPAS dedicated line list (Raspollini et al., 2013). Spectral features of the molecule BrONO<sub>2</sub> were calculated using new pressure–temperature-dependent absorption cross sections measured by Wagner and Birk (2016) with a 2% intensity accuracy. KOPRA also provides derivatives of the radiance spectrum with respect to atmospheric state and instrument parameters (Jacobians) which are used by the retrieval procedure KOPRAFIT (Höpfner et al., 2002). The vertical distance of tangent altitudes ranges between 1 and 1.5 km. Thus, the retrieval grid was set to 1 km up to the balloon float (observer) altitude. Above this level, the vertical spacing increases gradually up to 10 km at the top altitude of 100 km. Considering the smoothing of the vertical part of the instrumental field of view, the retrieval grid is somewhat finer than the achievable vertical resolution of the measurement for most parts of the altitude region covered (especially above the observer altitude). To avoid retrieval instabilities caused by this oversampling, a Tikhonov–Phillips regularization approach (Phillips, 1962; Tikhonov, 1963) was applied using a constraint with respect to a first derivative of the a priori profile  $x_a$  of the target species:

$$x_{i+1} = x_i + [\mathbf{K}_i^T \mathbf{S}_y^{-1} \mathbf{K}_i + \mathbf{R}]^{-1} [\mathbf{K}_i^T \mathbf{S}_y^{-1} (y_{\text{meas}} - y(x_i)) - \mathbf{R}(x_i - x_a)], \quad (1)$$

where  $x_{i+1}$  is the vector of the state parameters  $x_i$  for iteration  $i + 1$ ;  $y_{\text{meas}}$  is the measured radiance vector and  $y(x_i)$  the calculated radiance using state parameters of iteration  $i$ ;  $\mathbf{K}$  is the Jacobian matrix with partial derivatives  $\partial y(x_i)/\partial x_i$ , while  $\mathbf{S}_y^{-1}$  is the inverse noise measurement covariance matrix and  $\mathbf{R}$  a regularization matrix composed of the first-derivative operator and a regularization strength parameter.

The BrONO<sub>2</sub> retrieval calculations were performed in the range of the  $\nu_3$  band centred at 803.37 cm<sup>-1</sup>. Figure 1 shows spectral contributions of relevant species in the BrONO<sub>2</sub> micro-window from 801 to 820 cm<sup>-1</sup>, which has been found the most appropriate to derive the BrONO<sub>2</sub> amount from MIPAS-B spectra. Besides the target molecule BrONO<sub>2</sub>, all main interfering species H<sub>2</sub>O, CO<sub>2</sub>, O<sub>3</sub>, NO<sub>2</sub>, HNO<sub>3</sub>, COF<sub>2</sub>, HCFC-22 (CHClF<sub>2</sub>), CCl<sub>4</sub>, CFC-113 (C<sub>2</sub>Cl<sub>3</sub>F<sub>3</sub>), ClONO<sub>2</sub>, HO<sub>2</sub>NO<sub>2</sub>, and PAN (peroxyacetyl nitrate) were fitted simultaneously together with temperature, instrumental (radiometric) offset, and wavenumber shift. The molecule HO<sub>2</sub>NO<sub>2</sub> shows a similar spectral band shape like the target species BrONO<sub>2</sub>. Since the HO<sub>2</sub>NO<sub>2</sub> absorption cross sections (included in HITRAN) measured by May and Friedl (1993) are derived at only one temperature (220 K), a second set of cross sections derived by Friedl et al. (1994) at room temperature (298 K) was used to allow a two-point interpolation of the cross section intensity to the current atmospheric temperature.

Vertical profiles of minor contributing species were either adjusted in appropriate micro-windows prior to the BrONO<sub>2</sub> retrieval or taken from a climatological atmosphere (Remedios et al., 2007), updated with surface concentration data from NOAA ESRL GMD (National Oceanic and Atmospheric Administration, Earth System Research Laboratory,

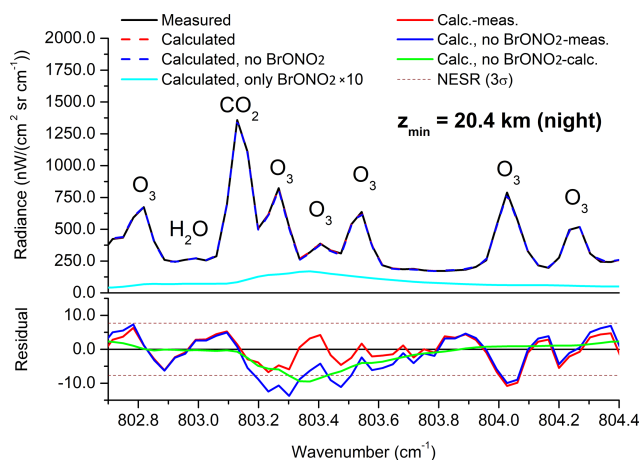


**Figure 2.** Top panel: best fit of measured spectrum (black solid line) zoomed around the  $Q$ -branch of the BrONO<sub>2</sub>  $\nu_3$  fundamental band at 803.37 cm<sup>-1</sup> for a tangent altitude ( $z_{\min}$ ) near 20 km recorded during the night on 7–8 September 2014 above Timmins (Seq. 05a). A calculation with (red dashed line) and without (blue dashed line) BrONO<sub>2</sub> in the model atmosphere was performed. The calculated individual emission of the BrONO<sub>2</sub> band (scaled by a factor of 10; cyan solid line) is also shown. Bottom panel: difference between the calculated and measured spectrum (red solid line); difference between the calculated spectrum (without BrONO<sub>2</sub>) and the measured one (blue solid line); difference of both calculations (green solid line). The  $3\sigma$  NESR (brown dotted line) is also displayed.

Global Monitoring Division; Montzka et al., 1999). An example of a best fit of a measured MIPAS-B spectrum zoomed around the  $Q$ -branch region of the BrONO<sub>2</sub>  $\nu_3$  band for a tangent altitude near 20 km is shown in Fig. 2. The spectrum was recorded during the night. If the fit is performed in the absence of BrONO<sub>2</sub> in the model atmosphere, a systematic residual remains around the centre of the BrONO<sub>2</sub>  $Q$ -branch at 803.37 cm<sup>-1</sup> (blue solid line in Fig. 2). If the molecule BrONO<sub>2</sub> is taken into account by the radiative transfer calculation, the systematic residual around the  $Q$ -branch disappears demonstrating the existence of BrONO<sub>2</sub> in the stratosphere. Another example of a best fit in the same altitude region but for a MIPAS-B spectrum recorded during the day is illustrated in Fig. 3. Here, we recognize that for a daytime situation the effect of whether the species BrONO<sub>2</sub> is included in the radiative transfer calculations or not is clearly smaller compared to the nighttime case (cf. Fig. 2) such that we expect lower-stratospheric BrONO<sub>2</sub> VMRs during the day and higher values at night. This is confirmed by the retrieved vertical profiles of BrONO<sub>2</sub> illustrated in Figs. 4 and 5 together with the error budget and altitude resolution. The dominant part of the total error in the BrONO<sub>2</sub> retrieval is spectral (random) noise resulting in a BrONO<sub>2</sub> VMR error of about 2 to 4 pptv (10–25%) in the altitude region of the VMR maximum. Uncertainties of disturbing gases overlapping the BrONO<sub>2</sub>  $\nu_3$  band are an important systematic error source. This influence was estimated using uncertainties in line in-

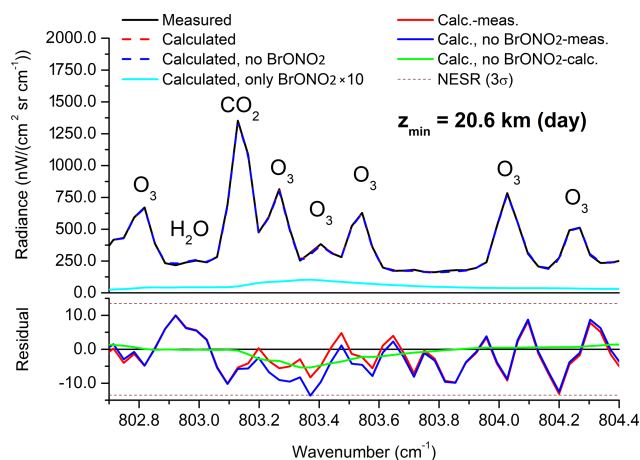


**Figure 3.** Same as Fig. 2 but for a spectrum observed during the day (Seq. 02e). The difference between the red and blue solid line (bottom panel) is smaller than the corresponding nighttime difference shown in Fig. 2. Hence, BrONO<sub>2</sub> amounts seen during the day are lower than the ones observed at night.

tensity and half-width as given by Flaud et al. (2003) and HITRAN (Rothman et al., 2009) and results into a BrONO<sub>2</sub> error of up to 2 pptv (10–20%) in the altitude region of the BrONO<sub>2</sub> VMR maximum. Retrieval simulations of the major interfering species O<sub>3</sub>, CO<sub>2</sub>, and H<sub>2</sub>O have revealed an influence (line half-width and intensity uncertainties) within 10% on the BrONO<sub>2</sub> amount (Höpfner et al., 2009). The species ClONO<sub>2</sub>, followed by HO<sub>2</sub>NO<sub>2</sub> have large contributions to the limb emission spectra (see Fig. 1). Temperature- and pressure-dependent ClONO<sub>2</sub> absorption cross sections were measured by Wagner and Birk (2003) with a high accuracy. Systematic errors in the BrONO<sub>2</sub> VMR due to ClONO<sub>2</sub> spectroscopy are expected to be within 10% (Wagner and Birk, 2016). As mentioned above, a temperature dependence of HO<sub>2</sub>NO<sub>2</sub> absorption cross sections was included to improve spectroscopy of this interfering species. Further systematic error sources like radiometric gain, line of sight, and the spectroscopy of the target molecule BrONO<sub>2</sub> itself are of minor importance for the total error budget of the BrONO<sub>2</sub> retrieval (see Figs. 4 and 5). The altitude resolution of the retrieved BrONO<sub>2</sub> profiles was calculated from the full width at half maximum (FWHM) of the rows of the averaging kernel matrix. It amounts to between about 4 and 6 km (~4–5 degrees of freedom) over a wide range in the stratosphere (see right column of Figs. 4 and 5).

### 2.3 Model calculations

Measured MIPAS-B data are compared to a multi-year simulation of the chemistry climate model EMAC, which includes sub-models describing tropospheric and middle atmosphere processes (Jöckel et al., 2010). The core atmospheric model is the fifth-generation European Centre Hamburg gen-

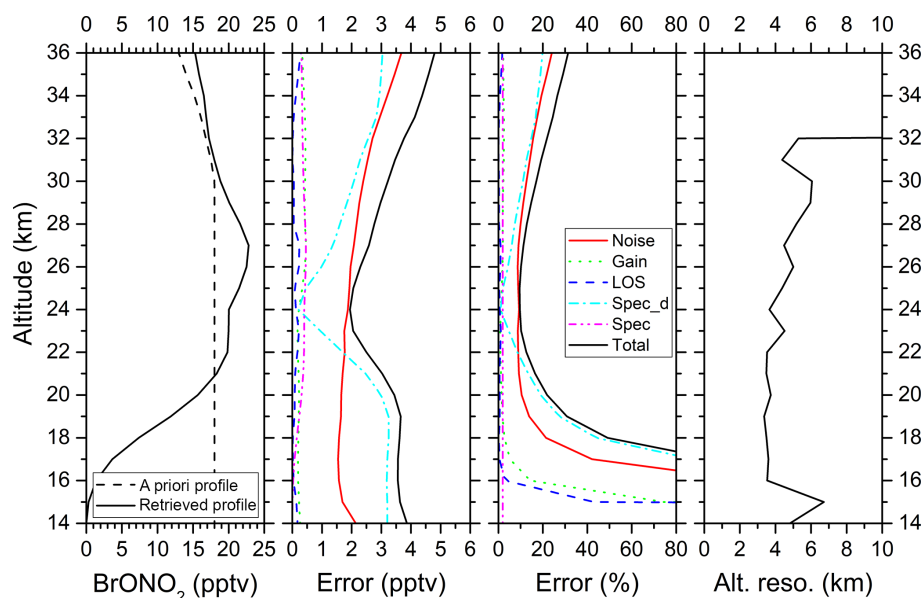


**Figure 4.** Retrieved BrONO<sub>2</sub> VMR vertical profile (and a priori profile) for a nighttime (Seq. 05a) limb sequence recorded by MIPAS-B on 7–8 September 2014 above Timmins together with absolute and relative errors and the altitude resolution, determined from the full width at half maximum of the rows of the averaging kernel matrix. The following error contributions are shown: spectral noise (red solid line), radiometric gain (green dotted line), LOS (line of sight) (blue dashed line), spectroscopic data of disturbing gases (dash–dotted cyan line), spectroscopic data of target molecule BrONO<sub>2</sub> (short dash–dotted magenta line), and total error (black solid line).

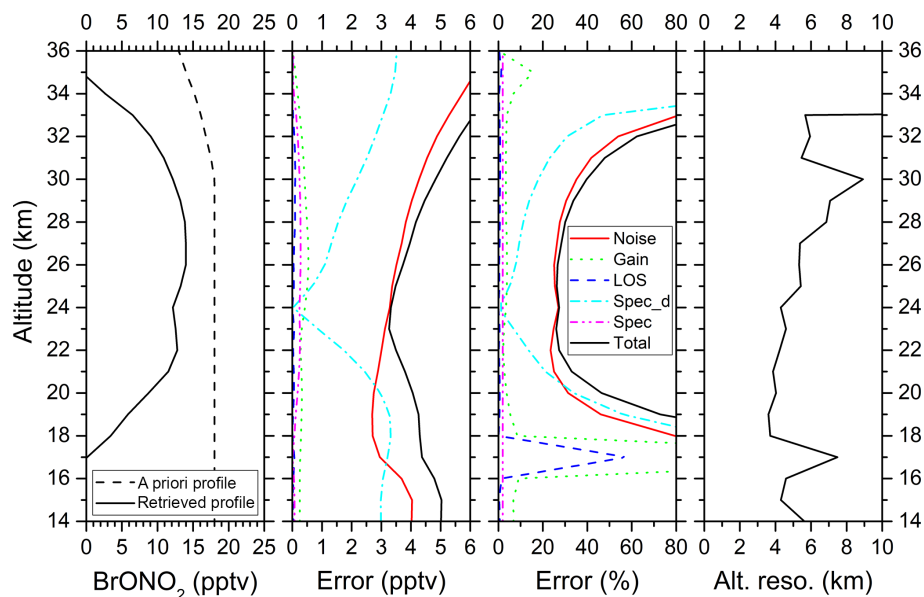


**Figure 5.** Same as Fig. 4 but for a limb sequence measured during the day (Seq. 02e).

eral circulation model (ECHAM5; Roeckner et al., 2006), which is linked to the sub-models via the interface Modular Earth Submodel System (MESSy). For the present study we applied EMAC (ECHAM5 version 5.3.02, MESSy version 2.52) in the T42L90MA-resolution, i.e., with a spherical truncation of T42 (corresponding to a Gaussian grid of approximately  $2.8 \times 2.8^\circ$  in latitude and longitude) and 90 ver-

tical hybrid pressure levels from the ground up to 0.01 hPa (approx. 80 km). The calculation of gas-phase chemistry is realized by the sub-model MECCA (Sander et al., 2005). The sub-model MSBM (Kirner et al., 2011) simulates polar stratospheric clouds and calculates heterogeneous reaction rates.

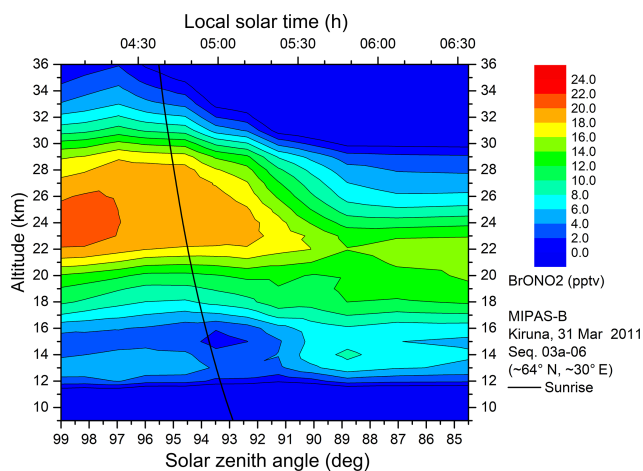


**Figure 6.** Temporal evolution of BrONO<sub>2</sub> volume mixing ratios (pptv) as seen by MIPAS-B from a float altitude around 35 km above northern Scandinavia on 31 March 2011 inside the late winter Arctic vortex. The black solid line marks the sunrise terminator. A decrease in the BrONO<sub>2</sub> amount starting around sunrise is clearly visible.

A Newtonian relaxation technique of the surface pressure and the prognostic variables temperature, vorticity, and divergence above the boundary layer and below 1 hPa towards the ECMWF reanalysis ERA-Interim (Dee et al., 2011) has been applied to simulate realistic synoptic conditions (van Aalst, 2005). The simulation includes a comprehensive chemistry set-up from the troposphere to the lower mesosphere with more than 100 species involved in gas-phase, photolysis, and heterogeneous reactions on liquid sulfate aerosols, nitric acid trihydrate (NAT), and ice particles. Rate constants of gas-phase reactions originate from Atkinson et al. (2007) and the Jet Propulsion Laboratory (JPL) compilation (Sander et al., 2011). Photochemical reactions of short-lived bromine-containing organic compounds CH<sub>3</sub>Br, CHBr<sub>3</sub>, CH<sub>2</sub>Br<sub>2</sub>, CH<sub>2</sub>ClBr, CHClBr<sub>2</sub>, and CHCl<sub>2</sub>Br are integrated into the model set-up (Jöckel et al., 2016). Surface emissions of these species are taken from scenario 5 of Warwick et al. (2006). During the time period with MIPAS-B balloon flights, the model output data were saved every 10 min. The temporally closest model output to the MIPAS-B measurements was interpolated in space to the observed geolocations.

### 3 Results and discussion

In this section, vertical profiles retrieved from MIPAS-B limb emission spectra measured before and after sunrise (Arctic flights) and sunset (midlatitude flight) are shown. The measured data have been temporally smoothed with a three-point adjacent averaging routine to attenuate noisy structures. These data were compared to EMAC simulations. To permit a more realistic comparison with respect to different altitude resolutions in the measurement and the simulation, EMAC

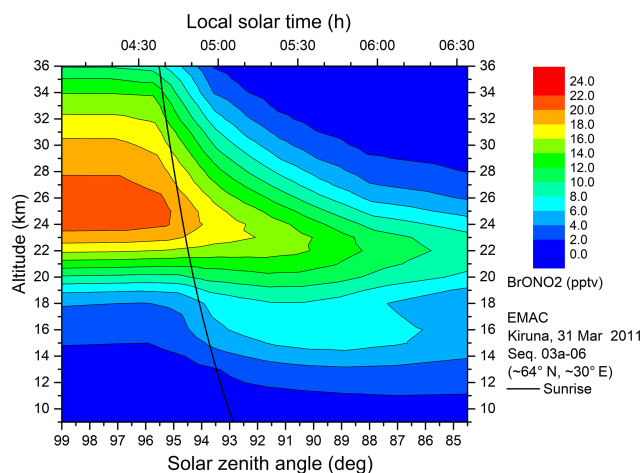


**Figure 7.** Temporal evolution of BrONO<sub>2</sub> on 31 March 2011 as simulated by the chemistry climate model EMAC. The decrease in BrONO<sub>2</sub> starts close to sunrise.

vertical profiles were additionally smoothed with the averaging kernel matrix and the a priori profile of MIPAS-B. A smoothed EMAC profile  $x_s$  is calculated following the method described in Rodgers (2000):

$$x_s = x_a + \mathbf{A} (x - x_a^*), \quad (2)$$

where  $x_a$  is the a priori profile of MIPAS-B,  $x_a^*$  the a priori profile interpolated to the altitude grid of the EMAC profile  $x$ , and  $\mathbf{A}$  is the averaging kernel matrix of MIPAS-B.

#### 3.1 Arctic measurements

The temporal evolution of BrONO<sub>2</sub> measured during the balloon flight from Kiruna on 31 March 2011 inside the late winter stratospheric polar vortex is shown in Fig. 6. No PSCs were present during the time of the MIPAS-B measurement (Wetzel et al., 2015). A nighttime maximum of BrONO<sub>2</sub> around 25 km with values of more than 20 pptv is clearly visible. After sunrise, the amount of BrONO<sub>2</sub> decreases to maximum values of about 14 pptv around 22 km. This downward displacement of the VMR maximum in terms of altitude can be explained by photolysis. Towards higher altitudes, the decomposition of BrONO<sub>2</sub> according to Reactions (R2a)–(R3) is increasingly faster than the BrONO<sub>2</sub> build-up via Reaction (R1). The overall structure (including the VMR altitude displacement) of the simulated temporal evolution of BrONO<sub>2</sub> is similar to the measured one and is shown in Fig. 7 together with the temporal development of the directly linked molecule BrO (Fig. 8). Maximum nighttime BrONO<sub>2</sub> values in EMAC are comparable to the measured amounts. However, above the nocturnal VMR maximum, EMAC calculates higher BrONO<sub>2</sub> concentrations compared to the balloon observation (see Fig. 9). Furthermore, the daytime photochemical destruction of BrONO<sub>2</sub> is slightly faster in the model, yielding several parts per trillion by volume lower daytime

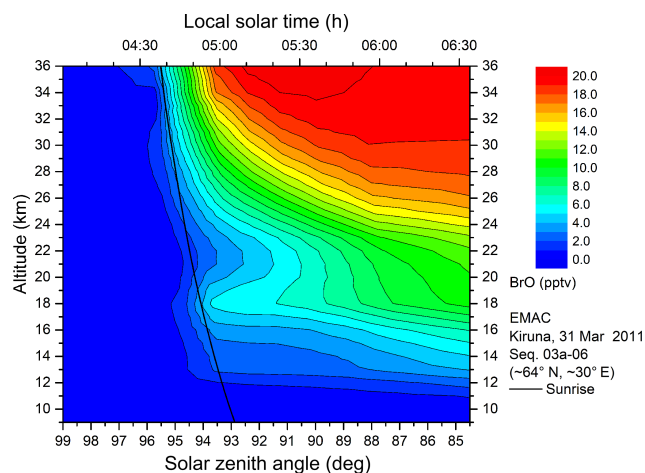


**Figure 8.** Temporal evolution of BrO on 31 March 2011 as simulated by the chemistry climate model EMAC. The opposite variation with BrONO<sub>2</sub> according to Reactions (R1)–(R3) is clearly visible.

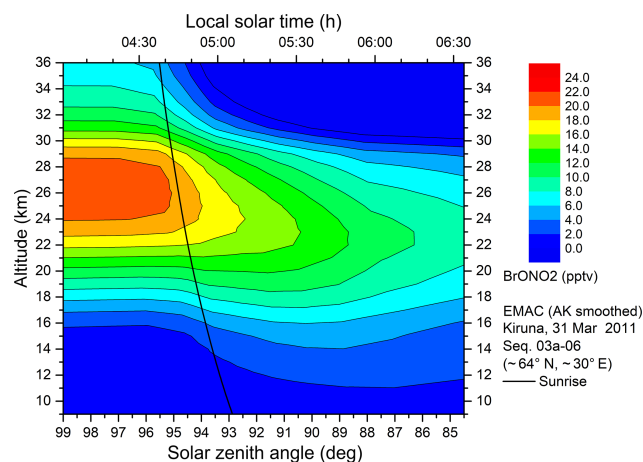


**Figure 10.** Same as Fig. 7 but EMAC vertical profiles smoothed with the MIPAS-B averaging kernel (AK).

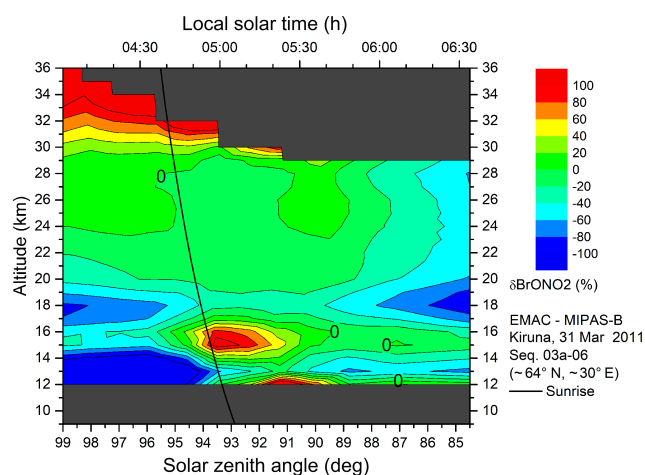


**Figure 9.** Relative BrONO<sub>2</sub> difference between EMAC and MIPAS-B in percent on 31 March 2011. Dark grey regions indicate MIPAS-B values less than 0.

BrONO<sub>2</sub> VMRs in the model compared to MIPAS-B. The EMAC simulation smoothed with the averaging kernel matrix of MIPAS-B according to Eq. (2) is displayed in Fig. 10. A main difference to the unsmoothed case shown in Fig. 7 is the reduction in the nighttime BrONO<sub>2</sub> VMR at altitudes above the maximum, which yields a better agreement with measured BrONO<sub>2</sub> (see Fig. 11).

Another Arctic balloon flight was performed from Kiruna on 24 January 2010 inside a cold polar vortex under midwinter weak illumination conditions. As a consequence of low stratospheric temperatures in this winter, widespread PSCs were present in an altitude region between about 18 and 24 km at the time of the MIPAS-B observation (Wetzel et al., 2012). The observed BrONO<sub>2</sub> as seen from night until noon is shown in Fig. 12. Nighttime BrONO<sub>2</sub> mixing ra-

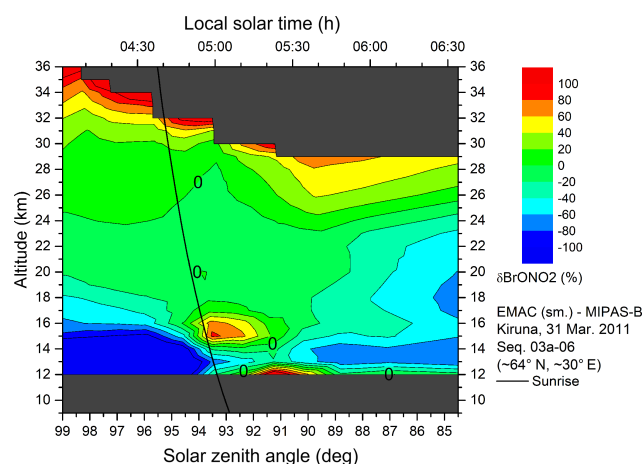


**Figure 11.** Relative BrONO<sub>2</sub> difference between EMAC (AK smoothed) and MIPAS-B in percent on 31 March 2011. Dark grey regions indicate MIPAS-B values less than 0.

tios are clearly lower compared to the previously discussed situation in late March 2011. This is also reflected in the EMAC simulation (Fig. 13) although there are some differences visible with regard to the observation (see Fig. 14). During the long polar night the amount of available NO<sub>2</sub> (Wetzel et al., 2012) to produce BrONO<sub>2</sub> via Reaction (R1) is significantly reduced due to the conversion of NO<sub>2</sub> into its reservoir species (mainly HNO<sub>3</sub>). In this period of darkness, nearly all BrONO<sub>2</sub> below 25 km (PSC region) is converted to BrCl via heterogeneous chemistry according to Reaction (R5) and gas-phase conversion of BrO to BrCl via Reaction (R6). Here, more than 90 % of Br<sub>y</sub> are in the form of BrCl in the model simulation during the night. Above this altitude region, BrONO<sub>2</sub> and BrCl together are the dominant species of the nocturnal Br<sub>y</sub> budget in the EMAC run. During the day, photolysis of both species (BrONO<sub>2</sub> and BrCl) leads to an increase in BrO such that this species then domi-

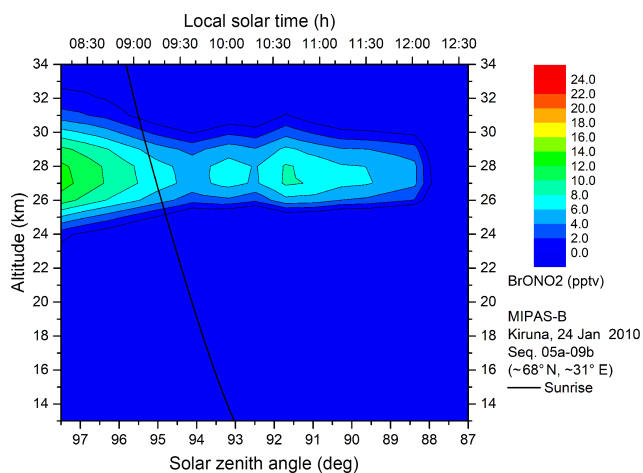


**Figure 12.** Temporal evolution of BrONO<sub>2</sub> volume mixing ratios (pptv) as measured by MIPAS-B on 24 January 2010 inside the midwinter Arctic vortex (observer altitude about 34 km). The black solid line marks the sunrise terminator. The still weak illumination at the end of the polar night is responsible for the small diurnal variation in the BrONO<sub>2</sub> amount.

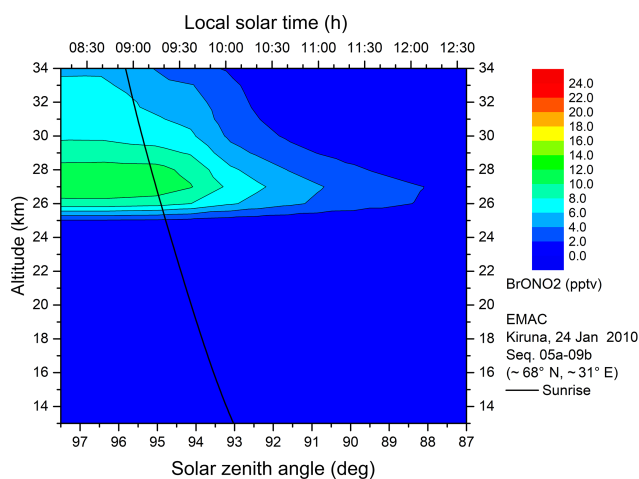


**Figure 13.** Temporal evolution of BrONO<sub>2</sub> on 24 January 2010 as simulated by the chemistry climate model EMAC. The decrease in BrONO<sub>2</sub> starts close to sunrise.

nates the Br<sub>y</sub> budget. If we smooth the EMAC BrONO<sub>2</sub> data with the averaging kernel matrix of MIPAS-B, we see a better agreement with MIPAS-B in the structure of the temporal evolution of the BrONO<sub>2</sub> amount (see Figs. 15 and 16). The effect of the smoothing appears to be stronger compared to the case in March 2011 since low temperatures together with low amounts of BrONO<sub>2</sub> in January 2010 meant performing the retrieval with a factor-of-2 coarser altitude resolution compared to a standard BrONO<sub>2</sub> retrieval set-up as depicted in Figs. 4 and 5.

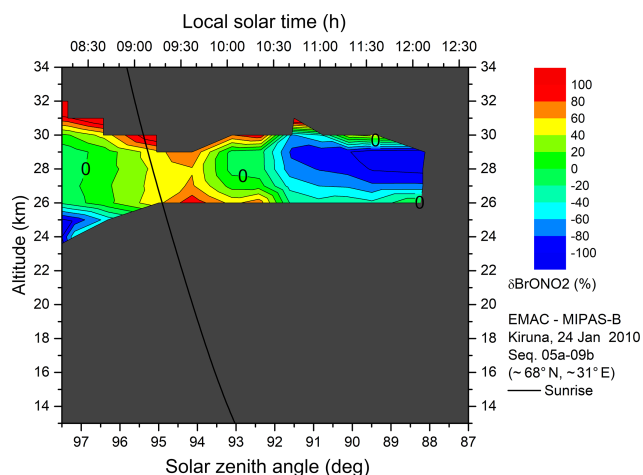


**Figure 14.** Relative BrONO<sub>2</sub> difference between EMAC and MIPAS-B in percent on 24 January 2010. Dark grey regions indicate MIPAS-B values less than 0.

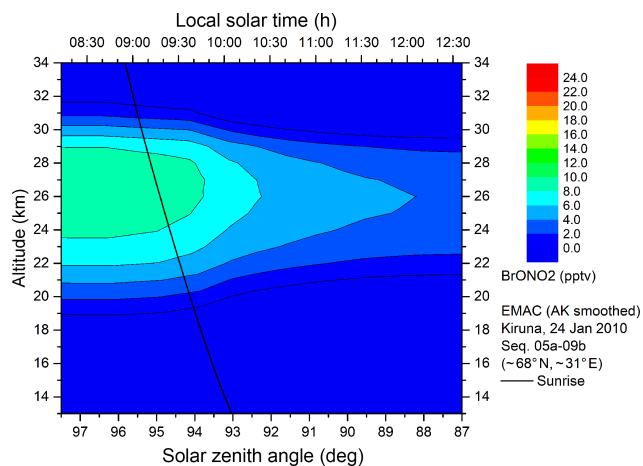


**Figure 15.** Same as Fig. 13 but EMAC vertical profiles smoothed with the MIPAS-B AK.

### 3.2 Midlatitude measurements

MIPAS-B spectra were recorded from day until night over Ontario (Canada) during a balloon flight launched from Timmins on 7 September 2014. The temporal evolution of measured BrONO<sub>2</sub> is depicted in Fig. 17. A significant increase in BrONO<sub>2</sub> starting shortly before sunset is visible. This is caused by the weakened illumination at solar zenith angles (SZAs) near 90°, which enables the build-up of BrONO<sub>2</sub> from daytime BrO via Reaction (R1). Nighttime BrONO<sub>2</sub> mixing ratios of more than 24 pptv are seen by MIPAS-B around 28 km altitude. The corresponding EMAC model simulation is displayed in Fig. 18. The principal shape of the increase in BrONO<sub>2</sub> VMR is reproduced by the model run although absolute values in the altitude region of the VMR maximum are somewhat lower in the simulation compared to the measurement (see Fig. 19). A sensitivity study



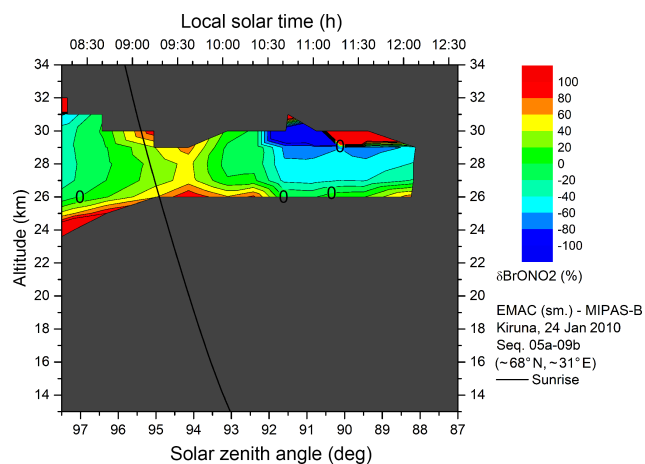


**Figure 16.** Relative BrONO<sub>2</sub> difference between EMAC (AK smoothed) and MIPAS-B in percent on 24 January 2010. Dark grey regions indicate MIPAS-B values less than 0.

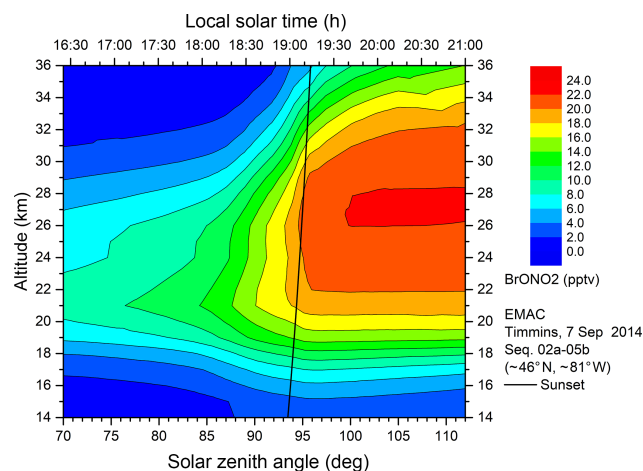


**Figure 18.** Temporal evolution of BrONO<sub>2</sub> on 7 September 2014 as simulated by the EMAC model.

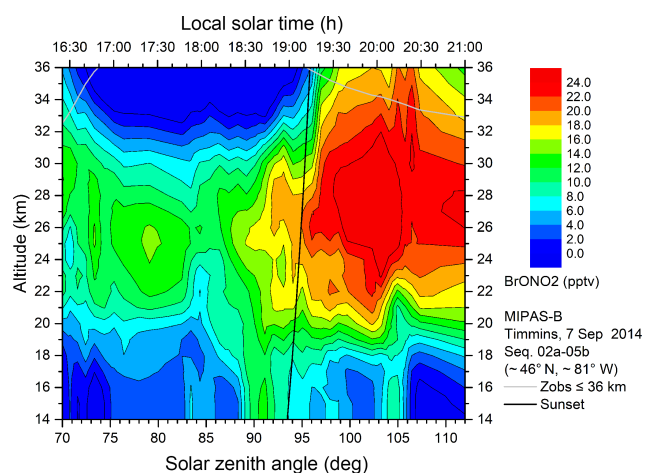


**Figure 17.** Temporal evolution of BrONO<sub>2</sub> amounts observed by MIPAS-B near 46° N above Ontario (Canada) on 7 September 2014. The grey line indicates the time periods in which the balloon gondola float altitude was lower or equal to 36 km. The black solid line marks the sunset terminator. The build-up of BrONO<sub>2</sub> from daytime BrO starts shortly before sunset.

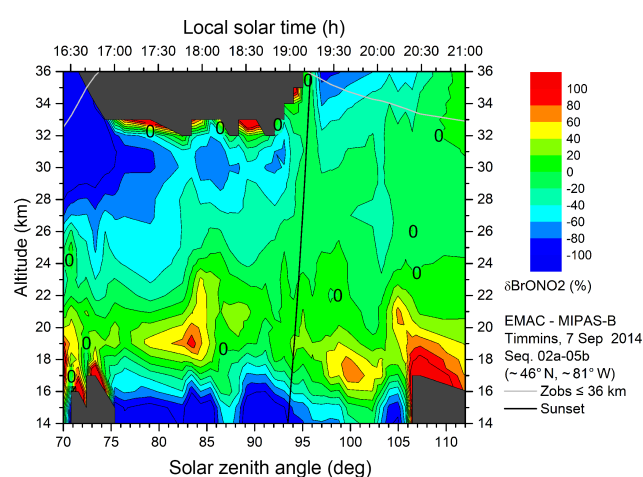


**Figure 19.** Relative BrONO<sub>2</sub> difference between EMAC and MIPAS-B in percent on 7 September 2014. Dark grey regions indicate MIPAS-B values less than 0.

based on measured BrO slant column densities performed by Kreycy et al. (2013) points to a possible stronger BrONO<sub>2</sub> photolysis rate and a lower reaction rate of the BrONO<sub>2</sub> build-up from BrO and NO<sub>2</sub> with respect to the JPL recommendation (Sander et al., 2011). However, our own sensitivity studies with a 1-D photochemical stacked box model (Sinnhuber et al., 2005) have shown that using the Kreycy et al. (2013) recommendation leads to lower BrONO<sub>2</sub> values during the day and towards higher BrO amounts and thus further degrades the agreement between model simulations and our MIPAS-B measurements. During the night, the simulated BrONO<sub>2</sub> VMR does not change significantly (< 0.1 pptv below 30 km). However, the Kreycy et al. (2013) study refers

to Arctic September conditions, and the outcome is therefore not directly comparable to the midlatitude observations shown here.

Differences in absolute BrONO<sub>2</sub> amounts between EMAC and MIPAS-B are at least partly connected with the fact that EMAC NO<sub>2</sub> values are up to 20 % lower than the observed NO<sub>2</sub> in the altitude region of the BrONO<sub>2</sub> VMR maximum. In the afternoon, the simulation already shows a weak temporal increase in BrONO<sub>2</sub> that is not seen by MIPAS-B. However, during the time of the strongest increase (18:30–19:20 LST), differences between EMAC and MIPAS-B are small (see Fig. 19). Nighttime maximum BrONO<sub>2</sub> values in EMAC reach about 22 pptv and are located in the same altitude region as seen in the observation. Smoothing the EMAC data with the averaging kernel matrix of MIPAS-B yields bet-

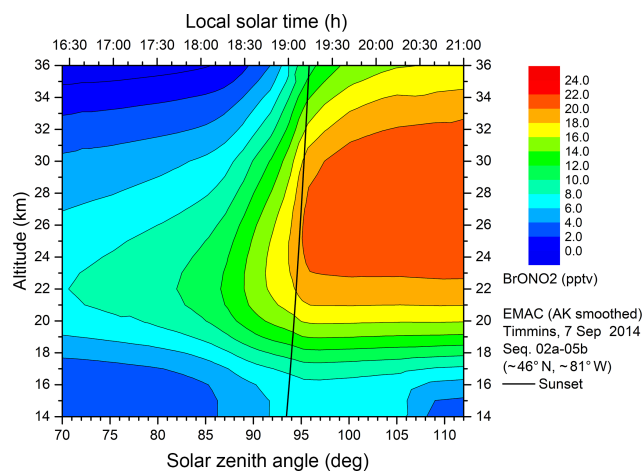


**Figure 20.** Same as Fig. 18 but EMAC vertical profiles smoothed with the MIPAS-B AK.

ter agreement with the structure of the observational data at altitudes below about 18 km (see Figs. 20 and 21).

### 3.3 Estimation of inorganic bromine

As already discussed in Sect. 1, BrONO<sub>2</sub> is a dominant species of lower-stratospheric inorganic bromine. Simulations with EMAC show that more than 90 % of nocturnal Br<sub>y</sub> is in the form of BrONO<sub>2</sub> between 21 and 29 km during the time of the MIPAS-B flight in September 2014. For comparison, the species BrO (not measurable by MIPAS-B) contributes no more than 80 % to total Br<sub>y</sub> during daytime in the altitude region of the MIPAS-B measurement). Furthermore, the concentration of BrO gradually changes during the day, while the amount of BrONO<sub>2</sub> is rather constant during nighttime. Hence, BrONO<sub>2</sub> is best suited to estimate the amount of “measured” inorganic bromine [Br<sub>y</sub>(meas)] from measured nighttime [BrONO<sub>2</sub>(meas)] using the calculated [BrONO<sub>2</sub>(mod)] / [Br<sub>y</sub>(mod)] ratio from EMAC in the following form:

$$[\text{Br}_y(\text{meas})] = \frac{[\text{BrONO}_2(\text{meas})][\text{Br}_y(\text{mod})]}{[\text{BrONO}_2(\text{mod})]} \quad (3)$$

We now apply Eq. (3) for the MIPAS-B midlatitude flight in September 2014 for a nighttime (SZA  $\geq 99^\circ$ ) ratio [BrONO<sub>2</sub>(mod)] / [Br<sub>y</sub>(mod)]  $\geq 0.9$  corresponding to an altitude region between 21 and 29 km. We then calculate [Br<sub>y</sub>(meas)] (including the total [BrONO<sub>2</sub>(meas)] error) to  $23.6 \pm 1.9$  pptv. The resulting error bar represents the  $1\sigma$  total error originating from measured BrONO<sub>2</sub>.

In the case of the Arctic flight in March 2011, the portion of BrONO<sub>2</sub> of total Br<sub>y</sub> is slightly smaller compared to the midlatitude situation. Applying Eq. (3) in an altitude region between 23 and 29 km, corresponding to a nighttime (SZA  $\geq 96^\circ$ ) ratio [BrONO<sub>2</sub>(mod)] / [Br<sub>y</sub>(mod)]  $\geq 0.8$ , we calculate [Br<sub>y</sub>(meas)] as being  $22.3 \pm 2.2$  pptv. An estima-

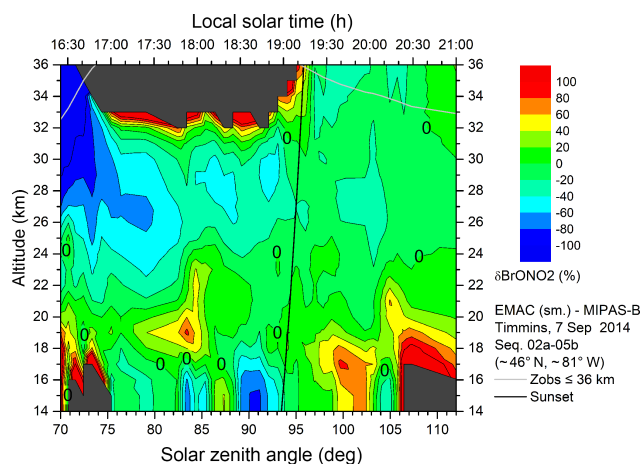


**Figure 21.** Relative BrONO<sub>2</sub> difference between EMAC (AK smoothed) and MIPAS-B in percent on 7 September 2014. Dark grey regions indicate MIPAS-B values less than 0.

tion of total Br<sub>y</sub> from the MIPAS-B data obtained during the Arctic flight in January 2010 is not reasonable since measured BrONO<sub>2</sub> values are very low during this time of the winter.

Our estimated Br<sub>y</sub> values can be compared to observations of stratospheric Br<sub>y</sub> calculated with photochemical modelling using balloon-borne direct-sun DOAS (differential optical absorption spectroscopy) BrO observations (Dorf et al., 2006; Carpenter et al., 2014) and annual mean mixing ratios derived from ground-based UV-visible measurements of stratospheric BrO (Sinnhuber et al., 2002; Hendrick et al., 2007, 2008; Carpenter et al., 2014). These observations show the temporal development of Br<sub>y</sub> depending on the year when air masses are entering the stratosphere. Assuming a mean age of air of 6 years at 25 km (Haenel et al., 2015), we can compare the measured Br<sub>y</sub> from MIPAS-B directly to the Br<sub>y</sub> from DOAS observations in the years (of stratospheric entry) 2005 and 2008. In these years, the range of expected Br<sub>y</sub> runs from about 18 to 25 pptv taking into account the error limits. Although the amount of Br<sub>y</sub> inferred from MIPAS-B measurements lies more towards the upper edge of this range, it is still consistent with the Br<sub>y</sub> estimates from DOAS observations.

## 4 Conclusions

BrONO<sub>2</sub> observations around sunrise and sunset were performed during balloon flights with MIPAS-B carried out in the Arctic from Kiruna on 24 January 2010 and 31 March 2011 and at midlatitudes from Timmins on 7–8 September 2014. Measured BrONO<sub>2</sub> diurnal variations with high nighttime and low daytime values confirm the stratospheric bromine chemistry (introduced in Sect. 1) that is dominated by the interaction of BrO and BrONO<sub>2</sub> ac-

according to Reactions (R1)–(R3). During polar winter (January 2010) with weak illumination, large parts of nighttime Br<sub>y</sub> are in the form of BrCl, resulting in significantly lower BrONO<sub>2</sub> values compared to the situation in late Arctic winter (March 2011) and midlatitude summer (September 2014).

The chemistry climate model EMAC is able to reproduce the temporal variation in the measured BrONO<sub>2</sub> values. However, some differences in the absolute amounts of BrONO<sub>2</sub> are obvious. The simulated BrONO<sub>2</sub> mixing ratios are dependent on the assumed total Br<sub>y</sub> in the model, which amounts to about 23 pptv in the lower stratosphere. As mentioned in Sect. 2.3 reactions of short-lived bromine-containing organic compounds are integrated into the model set-up according to emission scenarios shown by Warwick et al. (2006). This is equivalent to about 6–7 pptv inorganic bromine from these oceanic short-lived bromocarbons in the upper troposphere.

As discussed in Sect. 3.3, Br<sub>y</sub> in the lower stratosphere was estimated from MIPAS-B measurements. For the Arctic observation in March 2011, we obtain  $22.3 \pm 2.2$  pptv Br<sub>y</sub> and for the midlatitude measurement in September 2014, we calculate  $23.6 \pm 1.9$  pptv Br<sub>y</sub> in the lower stratosphere. These values are consistent with the range of Br<sub>y</sub> estimates from DOAS observations.

Finally, it should be mentioned that there is still some limited potential for the improvement of the spectroscopy of the interfering species (mainly HO<sub>2</sub>NO<sub>2</sub>) in the BrONO<sub>2</sub> spectral analysis window (Wagner and Birk, 2016). However, BrONO<sub>2</sub> test retrieval simulations for MIPAS-B (within this work) and MIPAS (Höpfner et al., 2009) have shown that future improvements in the spectroscopic database will most probably not exceed the total error limits given in this study.

*Data availability.* Please contact the leading author of this study.

*Competing interests.* The authors declare that they have no conflict of interest.

*Special issue statement.* This article is part of the special issue “Quadrennial Ozone Symposium 2016 – Status and trends of atmospheric ozone (ACP/AMT inter-journal SI)”. It is a result of the Quadrennial Ozone Symposium 2016, Edinburgh, UK, 4–9 September 2016.

*Acknowledgements.* We are grateful to the CNES balloon team for excellent balloon operations and the Swedish Space Corporation for operating Arctic campaigns and logistical assistance. We thank Katja Grunow from the Free University of Berlin for meteorological support. The work presented here was funded in part by the European Space Agency (ESA) and the German Aerospace Center (DLR). We acknowledge support by the Deutsche Forschungsgemeinschaft and Open Access Publishing

Fund of Karlsruhe Institute of Technology.

The article processing charges for this open-access publication were covered by a Research Centre of the Helmholtz Association.

Edited by: Sophie Godin-Beekmann

Reviewed by: two anonymous referees

## References

- Atkinson, R., Baulch, D. L., Cox, R. A., Crowley, J. N., Hampson, R. F., Hynes, R. G., Jenkin, M. E., Rossi, M. J., and Troe, J.: Evaluated kinetic and photochemical data for atmospheric chemistry: Volume III – gas phase reactions of inorganic halogens, *Atmos. Chem. Phys.*, 7, 981–1191, <https://doi.org/10.5194/acp-7-981-2007>, 2007.
- Brasseur, G. and Solomon, S.: *Aeronomy of the middle atmosphere*, in: *Atmos. Oceanograph. Sci. Lib.*, 3rd Edn., Springer, Dordrecht, the Netherlands, 369 pp., 2005.
- Carpenter, L. J., Reimann, S., Burkholder, J. B., Clerbaux, C., Hall, B. D., Hossaini, R., Laube, J. C., and Yvon-Lewis, S. A.: Ozone-Depleting Substances (ODSs) and other gases of interest to the Montreal Protocol, in: *Chapter 1 in Scientific Assessment of Ozone Depletion: 2014*, Global Ozone Research and Monitoring Project, Report No. 55, World Meteorological Organization, Geneva, Switzerland, 416 pp., 2014.
- Dee, D. P., Uppala, S. M., Simmons, A. J., Berrisford, P., Poli, P., Kobayashi, S., Andrae, U., Balmaseda, M. A., Balsamo, G., Bauer, P., Bechtold, P., Beljaars, A. C. M., van de Berg, L., Bidlot, J., Bormann, N., Delsol, C., Dragani, R., Fuentes, M., Geer, A. J., Haimberger, L., Healy, S. B., Hersbach, H., Hólm, E. V., Isaksen, I., Kållberg, P., Köhler, M., Matricardi, M., McNally, A. P., Monge-Sanz, B. M., Morcrette, J.-J., Park, B.-K., Peubey, C., deRosnay, P., Tavolato, C., Thépaut, J.-N., and Vitart, F.: The ERA-Interim reanalysis: configuration and performance of the data assimilation system, *Q. J. Roy. Meteorol. Soc.*, 137, 553–597, 2011.
- Dorf, M., Butler, J. H., Butz, A., Camy-Peyret, C., Chipperfield, M. P., Kritten, L., Montzka, S. A., Simmes, B., Weidner, F., and Pfeilsticker, K.: Long-term observations of stratospheric bromine reveal slow down in growth, *Geophys. Res. Lett.*, 33, L24803, <https://doi.org/10.1029/2006GL027714>, 2006.
- Flaud, J.-M., Piccolo, C., Carli, B., Perrin, A., Coudert, L. H., Teffo, J.-L., and Brown, L. R.: Molecular line parameters for the MIPAS (Michelson Interferometer for Passive Atmospheric Sounding) experiment, *Atmos. Ocean. Opt.*, 16, 172–182, 2003.
- Fiedl, R. R., May, R. D., and Duxbury, G.: The  $\nu_6$ ,  $\nu_7$ ,  $\nu_8$ , and  $\nu_{10}$  bands of HO<sub>2</sub>NO<sub>2</sub>, *J. Mol. Spectrosc.*, 165, 481–493, 1994.
- Fiedl-Vallon, F., Maucher, G., Kleinert, A., Lengel, A., Keim, C., Oelhaf, H., Fischer, H., Seefeldner, M., and Trieschmann, O.: Design and characterization of the balloon-borne Michelson Interferometer for Passive Atmospheric Sounding (MIPAS-B2), *Appl. Optics*, 43, 3335–3355, 2004.
- Haenel, F. J., Stiller, G. P., von Clarmann, T., Funke, B., Eckert, E., Glatthor, N., Grabowski, U., Kellmann, S., Kiefer, M., Linden, A., and Reddman, T.: Reassessment of MIPAS age of air

- trends and variability, *Atmos. Chem. Phys.*, 15, 13161–13176, <https://doi.org/10.5194/acp-15-13161-2015>, 2015.
- Hendrick, F., Van Roozendaal, M., Chipperfield, M. P., Dorf, M., Goutail, F., Yang, X., Fayt, C., Hermans, C., Pfeilsticker, K., Pommereau, J.-P., Pyle, J. A., Theys, N., and De Mazière, M.: Retrieval of stratospheric and tropospheric BrO profiles and columns using ground-based zenith-sky DOAS observations at Harestua, 60° N, *Atmos. Chem. Phys.*, 7, 4869–4885, <https://doi.org/10.5194/acp-7-4869-2007>, 2007.
- Hendrick, F., Johnston, P. V., De Mazière, M., Fayt, C., Hermans, C., Kreher, K., Theys, N., Thomas, A., and Van Roozendaal, M.: One-decade trend analysis of stratospheric BrO over Harestua (60° N) and Lauder (45° S) reveals a decline, *Geophys. Res. Lett.*, 35, L14801, <https://doi.org/10.1029/2008GL034154>, 2008.
- Höpfner, M., Oelhaf, H., Wetzel, G., Friedl-Vallon, F., Kleinert, A., Lengel, A., Maucher, G., Nordmeyer, H., Glatthor, N., Stiller, G., von Clarmann, T., Fischer, H., Kröger, C., and Deshler, T.: Evidence of scattering of tropospheric radiation by PSCs in mid-IR limb emission spectra: MIPAS-B observations and KOPRA simulations, *Geophys. Res. Lett.*, 29, 1278, <https://doi.org/10.1029/2001GL014443>, 2002.
- Höpfner, M., Orphal, J., von Clarmann, T., Stiller, G., and Fischer, H.: Stratospheric BrONO<sub>2</sub> observed by MIPAS, *Atmos. Chem. Phys.*, 9, 1735–1746, <https://doi.org/10.5194/acp-9-1735-2009>, 2009.
- Jöckel, P., Kerkweg, A., Pozzer, A., Sander, R., Tost, H., Riede, H., Baumgaertner, A., Gromov, S., and Kern, B.: Development cycle 2 of the Modular Earth Submodel System (MESSy2), *Geosci. Model Dev.*, 3, 717–752, <https://doi.org/10.5194/gmd-3-717-2010>, 2010.
- Jöckel, P., Tost, H., Pozzer, A., Kunze, M., Kirner, O., Brenninkmeijer, C. A. M., Brinkop, S., Cai, D. S., Dyroff, C., Eckstein, J., Frank, F., Garny, H., Gottschaldt, K.-D., Graf, P., Grewe, V., Kerkweg, A., Kern, B., Matthes, S., Mertens, M., Meul, S., Neumaier, M., Nützel, M., Oberländer-Hayn, S., Ruhnke, R., Runde, T., Sander, R., Scharffe, D., and Zahn, A.: Earth System Chemistry integrated Modelling (ESCI-Mo) with the Modular Earth Submodel System (MESSy) version 2.51, *Geosci. Model Dev.*, 9, 1153–1200, <https://doi.org/10.5194/gmd-9-1153-2016>, 2016.
- Kirner, O., Ruhnke, R., Buchholz-Dietsch, J., Jöckel, P., Brühl, C., and Steil, B.: Simulation of polar stratospheric clouds in the chemistry-climate-model EMAC via the submodel PSC, *Geosci. Model Dev.*, 4, 169–182, <https://doi.org/10.5194/gmd-4-169-2011>, 2011.
- Kleinert, A.: Correction of detector nonlinearity for the balloon-borne Michelson Interferometer for Passive Atmospheric Sounding, *Appl. Optics*, 45, 425–431, 2006.
- Kreycy, S., Camy-Peyret, C., Chipperfield, M. P., Dorf, M., Feng, W., Hossaini, R., Kritten, L., Werner, B., and Pfeilsticker, K.: Atmospheric test of the  $J(\text{BrONO}_2)/k_{\text{BrO}+\text{NO}_2}$  ratio: implications for total stratospheric Br<sub>y</sub> and bromine-mediated ozone loss, *Atmos. Chem. Phys.*, 13, 6263–6274, <https://doi.org/10.5194/acp-13-6263-2013>, 2013.
- May, R. D. and Friedl, R. R.: Integrated band intensities of HO<sub>2</sub>NO<sub>2</sub> at 220 K, *J. Quant. Spectrosc. Ra.*, 50, 257–266, 1993.
- Montzka, S. A., Butler, J. H., Elkins, J. W., Thompson, T. M., Clarke, A. D. and Lock, L. T.: Present and future trends in the atmospheric burden of ozone-depleting halogens, *Nature*, 398, 690–694, 1999.
- Newman, P. A., Daniel, J. S., Waugh, D. W., and Nash, E. R.: A new formulation of equivalent effective stratospheric chlorine (EESC), *Atmos. Chem. Phys.*, 7, 4537–4552, <https://doi.org/10.5194/acp-7-4537-2007>, 2007.
- Norton, H. and Beer, R.: New apodization functions for Fourier spectroscopy, *J. Opt. Soc. Am.*, 66, 259–264 (Errata, *J. Opt. Soc. Am.*, 67, 419, 1977.), 1976.
- Phillips, D.: A technique for the numerical solution of certain integral equations of the first kind, *J. Assoc. Comput. Math.*, 9, 84–97, 1962.
- Raspollini, P., Carli, B., Carlotti, M., Ceccherini, S., Dehn, A., Dinelli, B. M., Dudhia, A., Flaud, J.-M., López-Puertas, M., Niro, F., Remedios, J. J., Ridolfi, M., Sembhi, H., Sgheri, L., and von Clarmann, T.: Ten years of MIPAS measurements with ESA Level 2 processor V6 – Part I: Retrieval algorithm and diagnostics of the products, *Atmos. Meas. Tech.*, 6, 2419–2439, <https://doi.org/10.5194/amt-6-2419-2013>, 2013.
- Remedios, J. J., Leigh, R. J., Waterfall, A. M., Moore, D. P., Sembhi, H., Parkes, I., Greenhough, J., Chipperfield, M. P., and Hauglustaine, D.: MIPAS reference atmospheres and comparisons to V4.61/V4.62 MIPAS level 2 geophysical data sets, *Atmos. Chem. Phys. Discuss.*, 7, 9973–10017, <https://doi.org/10.5194/acpd-7-9973-2007>, 2007.
- Rodgers, C.: Inverse methods for atmospheric sounding: Theory and practice, World Sci., Hackensack, NJ, 2000.
- Roeckner, E., Brokopf, R., Esch, M., Giorgetta, M., Hagemann, S., Koernblueh, L., Manzini, E., Schlese, U., and Schulzweida, U.: Sensitivity of simulated climate to horizontal and vertical resolution in the ECHAM5 atmosphere model, *J. Climate*, 19, 3771–3791, 2006.
- Rothman, L. S., Gordon, I. E., Barbe, A., Benner, D. C., Bernath, P. F., Birk, M., Boudon, V., Brown, L. R., Campargue, A., Champion, J.-P., Chance, K., Coudert, L. H., Dana, V., Devi, V. M., Fally, S., Flaud, J.-M., Gamache, R. R., Goldman, A., Jacquemart, D., Kleiner, I., Lacome, N., Lafferty, W. J., Mandin, J.-Y., Massie, S. T., Mikhailenko, S. N., Miller, C. E., Moazzen-Ahmadi, N., Naumenko, O. V., Nikitin, A. V., Orphal, J., Perevalov, V. I., Perrin, A., Predoi-Cross, A., Rinsland, C. P., Rotger, M., Šimečková, M., Smith, M. A. H., Sung, K., Tashkun, S. A., Tennyson, J., Toth, R. A., Vandaele, A. C., and Vander Auwera, J.: The HITRAN 2008 molecular spectroscopic database, *J. Quant. Spectrosc. Ra.*, 110, 533–572, <https://doi.org/10.1016/j.jqsrt.2009.02.013>, 2009.
- Sander, R., Kerkweg, A., Jöckel, P., and Lelieveld, J.: Technical note: The new comprehensive atmospheric chemistry module MECCA, *Atmos. Chem. Phys.*, 5, 445–450, <https://doi.org/10.5194/acp-5-445-2005>, 2005.
- Sander, S. P., Friedl, R. R., Barker, J. R., Golden, D. M., Kurylo, M. J., Wine, P. H., Abbatt, J., Burkholder, J. B., Kolb, C. E., Moortgat, G. K., Huie, R. E., and Orkin, V. L.: Chemical kinetics and photochemical data for use in atmospheric studies, Evaluation no. 17, JPL Publ. 10-6, Jet Propulsion Laboratory, Pasadena, CA, 2011.
- Sinnhuber, B.-M. and Meul, S.: Simulating the impact of emissions of brominated very short lived substances on past stratospheric ozone trends, *Geophys. Res. Lett.*, 42, 2449–2456, <https://doi.org/10.1002/2014GL062975>, 2015.
- Sinnhuber, B.-M., Arlander, D. W., Bovensmann, H., Burrows, J. P., Chipperfield, M. P., Enell, C. F., Frieß, U., Hendrick, F.,

- Johnston, P. V., Jones, R. L., Kreher, K., Mohamed-Tahrin, N., Müller, R., Pfeilsticker, K., Platt, U., Pommereau, J.-P., Pundt, I., Richter, A., South, A. M., Tørnkvist, K. K., Van Roozendael, M., Wagner, T., and Wittrock, F.: Comparison of measurements and model calculations of stratospheric bromine monoxide, *J. Geophys. Res.*, 107, 4398, <https://doi.org/10.1029/2001JD000940>, 2002.
- Sinnhuber, B.-M., Rozanov, A., Sheode, N., Afe, O. T., Richter, A., Sinnhuber, M., Wittrock, F., Burrows, J. P., Stiller, G. P., von Clarmann, T., and Linden, A.: Global observations of stratospheric bromine monoxide from SCIAMACHY, *Geophys. Res. Lett.*, 32, L20810, <https://doi.org/10.1029/2005GL023839>, 2005.
- Sinnhuber, B.-M., Sheode, N., Sinnhuber, M., Chipperfield, M. P., and Feng, W.: The contribution of anthropogenic bromine emissions to past stratospheric ozone trends: a modelling study, *Atmos. Chem. Phys.*, 9, 2863–2871, <https://doi.org/10.5194/acp-9-2863-2009>, 2009.
- Stiller, G. P., von Clarmann, T., Funke, B., Glatthor, N., Hase, F., Höpfner, M., and Linden, A.: Sensitivity of trace gas abundances retrievals from infrared limb emission spectra to simplifying approximations in radiative transfer modeling, *J. Quant. Spectrosc. Ra.*, 72, 249–280, 2002.
- Stolarski, R. S., Douglass, A. R., Newman, P. A., Pawson, P., and Schoeberl, M. R.: Relative contribution of greenhouse gases and ozone-depleting substances to temperature trends in the stratosphere: A Chemistry-Climate Model study, *J. Climate*, 23, 28–42, 2010.
- Tikhonov, A.: On the solution of incorrectly stated problems and a method of regularization, *Dokl. Acad. Nauk SSSR*, 151, 501–504, 1963.
- van Aalst, M. K.: Dynamics and Transport in the Stratosphere – simulations with a general circulation model, PhD thesis, Institute for Marine and Atmospheric Research, Utrecht, the Netherlands, 2005.
- Wagner, G. and Birk, M.: New infrared spectroscopic database for chlorine nitrate, *J. Quant. Spectrosc. Ra.*, 82, 443–460, 2003.
- Wagner, G. and Birk, M.: New infrared spectroscopic database for bromine nitrate, *J. Mol. Spectrosc.*, 326, 95–105, 2016.
- Warwick, N. J., Pyle, J. A., Carver, G. D., Yang, X., Savage, N. H., O'Connor, F. M., and Cox, R. A.: Global modeling of biogenic bromocarbons, *J. Geophys. Res.*, 111, D24305, <https://doi.org/10.1029/2006JD007264>, 2006.
- Wetzel, G., Oelhaf, H., Kirner, O., Friedl-Vallon, F., Ruhnke, R., Ebersoldt, A., Kleinert, A., Maucher, G., Nordmeyer, H., and Orphal, J.: Diurnal variations of reactive chlorine and nitrogen oxides observed by MIPAS-B inside the January 2010 Arctic vortex, *Atmos. Chem. Phys.*, 12, 6581–6592, <https://doi.org/10.5194/acp-12-6581-2012>, 2012.
- Wetzel, G., Oelhaf, H., Birk, M., de Lange, A., Engel, A., Friedl-Vallon, F., Kirner, O., Kleinert, A., Maucher, G., Nordmeyer, H., Orphal, J., Ruhnke, R., Sinnhuber, B.-M., and Vogt, P.: Partitioning and budget of inorganic and organic chlorine species observed by MIPAS-B and TELIS in the Arctic in March 2011, *Atmos. Chem. Phys.*, 15, 8065–8076, <https://doi.org/10.5194/acp-15-8065-2015>, 2015.